



Testing Hadronic Interactions at Ultrahigh Energies with Air Showers Measured by the Pierre Auger Observatory

A. Aab,¹ P. Abreu,² M. Aglietta,^{3,4} E. J. Ahn,⁵ I. Al Samarai,⁶ I. F. M. Albuquerque,⁷ I. Allekotte,⁸ J. D. Allen,⁹ P. Allison,¹⁰ A. Almela,^{11,12} J. Alvarez Castillo,¹³ J. Alvarez-Muñiz,¹⁴ M. Ambrosio,¹⁵ G. A. Anastasi,¹⁶ L. Anchordoqui,¹⁷ B. Andrada,¹¹ S. Andringa,² C. Aramo,¹⁵ F. Arqueros,¹⁸ N. Arsene,¹⁹ H. Asorey,^{8,20} P. Assis,² J. Aublin,⁶ G. Avila,^{21,22} A. M. Badescu,²³ C. Baus,²⁴ J. J. Beatty,¹⁰ K. H. Becker,²⁵ J. A. Bellido,²⁶ C. Berat,²⁷ M. E. Bertaina,^{28,4} X. Bertou,⁸ P. L. Biermann,²⁹ P. Billoir,⁶ J. Biteau,³⁰ S. G. Blaess,²⁶ A. Blanco,² J. Blazek,³¹ C. Bleve,^{32,33} H. Blümer,^{24,34} M. Boháčová,³¹ D. Boncioli,^{35,†} C. Bonifazi,³⁶ N. Borodai,³⁷ A. M. Botti,^{11,34} J. Brack,³⁸ I. Brancus,³⁹ T. Bretz,⁴⁰ A. Bridgeman,³⁴ F. L. Briechle,⁴⁰ P. Buchholz,¹ A. Bueno,⁴¹ S. Buitink,⁴² M. Buscemi,^{43,44} K. S. Caballero-Mora,⁴⁵ B. Caccianiga,⁴⁶ L. Caccianiga,⁶ A. Cancio,^{12,11} F. Canfora,⁴² L. Caramete,⁴⁷ R. Caruso,^{43,44} A. Castellina,^{3,4} G. Cataldi,³³ L. Cazon,² R. Cester,^{28,4} A. G. Chavez,⁴⁸ A. Chiavassa,^{28,4} J. A. Chinellato,⁴⁹ J. C. Chirinos Diaz,⁵⁰ J. Chudoba,³¹ R. W. Clay,²⁶ R. Colalillo,^{51,15} A. Coleman,⁵² L. Collica,⁴ M. R. Coluccia,^{32,33} R. Conceição,² F. Contreras,^{21,22} M. J. Cooper,²⁶ S. Coutu,⁵² C. E. Covault,⁵³ J. Cronin,⁵⁴ R. Dallier,^{55,56} S. D'Amico,^{57,33} B. Daniel,⁴⁹ S. Dasso,^{58,59} K. Daumiller,³⁴ B. R. Dawson,²⁶ R. M. de Almeida,⁶⁰ S. J. de Jong,^{42,61} G. De Mauro,⁴² J. R. T. de Mello Neto,³⁶ I. De Mitri,^{32,33} J. de Oliveira,⁶⁰ V. de Souza,⁶² J. Debatin,³⁴ L. del Peral,⁶³ O. Deligny,³⁰ N. Dhital,⁵⁰ C. Di Giulio,^{64,65} A. Di Matteo,^{66,16} M. L. Díaz Castro,⁴⁹ F. Diogo,² C. Dobrigkeit,⁴⁹ J. C. D'Olivo,¹³ A. Dorofeev,¹³ R. C. dos Anjos,⁶⁷ M. T. Dova,⁶⁸ A. Dundovic,⁶⁹ J. Ebr,³¹ R. Engel,³⁴ M. Erdmann,⁴⁰ M. Erfani,¹ C. O. Escobar,^{5,49} J. Espadanal,² A. Etchegoyen,^{11,12} H. Falcke,^{42,70,61} K. Fang,⁵⁴ G. R. Farrar,⁹ A. C. Fauth,⁴⁹ N. Fazzini,⁵ A. P. Ferguson,⁵³ B. Fick,⁵⁰ J. M. Figueira,¹¹ A. Filevich,¹¹ A. Filipčič,^{71,72} O. Fratu,²³ M. M. Freire,⁷³ T. Fujii,⁵⁴ A. Fuster,^{11,12} F. Gallo,¹¹ B. García,⁷⁴ D. Garcia-Pinto,¹⁸ F. Gate,⁵⁵ H. Gemmeke,⁷⁵ A. Gherghel-Lascu,³⁹ P. L. Ghia,⁶ U. Giaccari,³⁶ M. Giammarchi,⁴⁶ M. Giller,⁷⁶ D. Głás,⁷⁶ C. Glaser,⁴⁰ H. Glass,⁵ G. Golup,⁸ M. Gómez Berisso,⁸ P. F. Gómez Vitale,^{21,22} N. González,^{11,34} B. Gookin,³⁸ J. Gordon,¹⁰ A. Gorgi,^{3,4} P. Gorham,⁷⁷ P. Gouffon,⁷ N. Griffith,¹⁰ A. F. Grillo,³⁵ T. D. Grubb,²⁶ F. Guarino,^{51,15} G. P. Guedes,⁷⁸ M. R. Hampel,¹¹ P. Hansen,⁶⁸ D. Harari,⁸ T. A. Harrison,²⁶ J. L. Harton,³⁸ Q. Hasankiadeh,³⁴ A. Haungs,³⁴ T. Hebbeker,⁴⁰ D. Heck,³⁴ P. Heimann,¹ A. E. Herve,²⁴ G. C. Hill,²⁶ C. Hojvat,⁵ N. Hollon,⁵⁴ E. Holt,^{34,11} P. Homola,³⁷ J. R. Hörandel,^{42,61} P. Horvath,⁷⁹ M. Hrabovský,⁷⁹ T. Huege,³⁴ J. Hulsman,^{11,34} A. Insolia,^{43,44} P. G. Isar,⁴⁷ I. Jandt,²⁵ S. Jansen,^{42,61} C. Jarne,⁶⁸ J. A. Johnsen,⁸⁰ M. Josebachuili,¹¹ A. Kääpä,²⁵ O. Kambeitz,²⁴ K. H. Kampert,²⁵ P. Kasper,⁵ I. Katkov,²⁴ B. Keilhauer,³⁴ E. Kemp,⁴⁹ R. M. Kieckhafer,⁵⁰ H. O. Klages,³⁴ M. Kleifges,⁷⁵ J. Kleinfeller,²¹ R. Krause,⁴⁰ N. Krohm,²⁵ D. Kuempel,⁴⁰ G. Kukec Mezek,⁷² N. Kunka,⁷⁵ A. Kuotb Awad,³⁴ D. LaHurd,⁵³ L. Latronico,⁴ M. Lauscher,⁴⁰ P. Lautridou,⁵⁵ P. Lebrun,⁵ R. Legumina,⁷⁶ M. A. Leigui de Oliveira,⁸¹ A. Letessier-Selvon,⁶ I. Lhenry-Yvon,³⁰ K. Link,²⁴ L. Lopes,² R. López,⁸² A. López Casado,¹⁴ A. Lucero,^{11,12} M. Malacari,²⁶ M. Mallamaci,^{83,46} D. Mandat,³¹ P. Mantsch,⁵ A. G. Mariuzzi,⁶⁸ V. Marin,⁵⁵ I. C. Mariş,⁴¹ G. Marsella,^{32,33} D. Martello,^{32,33} H. Martinez,⁸⁴ O. Martínez Bravo,⁸² J. J. Masías Meza,⁵⁹ H. J. Mathes,³⁴ S. Mathys,²⁵ J. Matthews,⁸⁵ J. A. J. Matthews,⁸⁶ G. Matthiae,^{64,65} D. Maurizio,⁸⁷ E. Mayotte,⁸⁰ P. O. Mazur,⁵ C. Medina,⁸⁰ G. Medina-Tanco,¹³ V. B. B. Mello,³⁶ D. Melo,¹¹ A. Menshikov,⁷⁵ S. Messina,⁸⁸ M. I. Micheletti,⁷³ L. Middendorf,⁴⁰ I. A. Minaya,¹⁸ L. Miramonti,^{83,46} B. Mitrica,³⁹ L. Molina-Bueno,⁴¹ S. Mollerach,⁸ F. Montanet,²⁷ C. Morello,^{3,4} M. Mostafá,⁵² C. A. Moura,⁸¹ G. Müller,⁴⁰ M. A. Muller,^{49,89} S. Müller,^{34,11} I. Naranjo,⁸ S. Navas,⁴¹ P. Necsai,³¹ L. Nellen,¹³ A. Nelles,^{42,61} J. Neuser,²⁵ P. H. Nguyen,²⁶ M. Niculescu-Oglinzanu,³⁹ M. Niechciol,¹ L. Niemietz,²⁵ T. Niggemann,⁴⁰ D. Nitz,⁵⁰ D. Nosek,⁹⁰ V. Novotny,⁹⁰ H. Nožka,⁷⁹ L. A. Núñez,²⁰ L. Ochilo,¹ F. Oikonomou,⁵² A. Olinto,⁵⁴ D. Pakk Selmi-Dei,⁴⁹ M. Palatka,³¹ J. Pallotta,⁹¹ P. Papenbreer,²⁵ G. Parente,¹⁴ A. Parra,^{92,17} T. Paul,^{92,17} M. Pech,³¹ F. Pedreira,¹⁴ J. Pečala,³⁷ R. Pelayo,⁹³ J. Peña-Rodríguez,²⁰ I. M. Pepe,⁹⁴ L. A. S. Pereira,⁴⁹ L. Perrone,^{32,33} E. Petermann,⁹⁵ C. Peters,⁴⁰ S. Petrera,^{66,16} J. Phuntsok,⁵² R. Piegaiia,⁵⁹ T. Pierog,³⁴ P. Pieroni,⁵⁹ M. Pimenta,² V. Pirronello,^{43,44} M. Platino,¹¹ M. Plum,⁴⁰ C. Porowski,³⁷ R. R. Prado,⁶² P. Privitera,⁵⁴ M. Prouza,³¹ E. J. Quel,⁹¹ S. Querschfeld,²⁵ S. Quinn,⁵³ J. Rautenberg,²⁵ O. Ravel,⁵⁵ D. Ravignani,¹¹ B. Revenu,⁵⁵ J. Ridky,³¹ M. Risse,¹ P. Ristori,⁹¹ V. Rizi,^{66,16} W. Rodrigues de Carvalho,¹⁴ J. Rodríguez Rojo,²¹ M. D. Rodríguez-Frías,⁶³ D. Rogozin,³⁴ J. Rosado,¹⁸ M. Roth,³⁴ E. Roulet,⁸ A. C. Rovero,⁵⁸ S. J. Saffi,²⁶ A. Saftoiu,³⁹ H. Salazar,⁸² A. Saleh,⁷² F. Salesa Greus,⁵² G. Salina,⁶⁵ J. D. Sanabria Gomez,²⁰ F. Sánchez,¹¹ P. Sanchez-Lucas,⁴¹ E. M. Santos,⁷ E. Santos,⁴⁹ F. Sarazin,⁸⁰ B. Sarkar,²⁵ R. Sarmiento,² C. Sarmiento-Cano,²⁰ R. Sato,²¹ C. Scarso,²¹ M. Schauer,²⁵ V. Scherini,^{32,33} H. Schieler,³⁴ D. Schmidt,^{34,11} O. Scholten,^{88,‡} H. Schoorlemmer,⁷⁷ P. Schovánek,³¹ F. G. Schröder,³⁴ A. Schulz,³⁴ J. Schulz,⁴² J. Schumacher,⁴⁰ S. J. Sciutto,⁶⁸ A. Segreto,^{96,44} M. Settimo,⁶ A. Shadkam,⁸⁵ R. C. Shellard,⁸⁷ G. Sigl,⁶⁹ O. Sima,¹⁹ A. Śmiałkowski,⁷⁶ R. Šmída,³⁴ G. R. Snow,⁹⁵ P. Sommers,⁵² S. Sonntag,¹ J. Sorokin,²⁶ R. Squartini,²¹ D. Stanca,³⁹ S. Stanič,⁷² J. Stapleton,¹⁰

J. Stasielak,³⁷ F. Strafella,^{32,33} A. Stutz,²⁷ F. Suarez,^{11,12} M. Suarez Durán,²⁰ T. Sudholz,²⁶ T. Suomijärvi,³⁰ A. D. Supanitsky,⁵⁸ M. S. Sutherland,¹⁰ J. Swain,⁹² Z. Szadkowski,⁷⁶ O. A. Taborda,⁸ A. Tapia,¹¹ A. Tepe,¹ V. M. Theodoro,⁴⁹ C. Timmermans,^{61,42} C. J. Todero Peixoto,⁹⁷ L. Tomankova,³⁴ B. Tomé,² A. Tonachini,^{28,4} G. Torralba Elipe,¹⁴ D. Torres Machado,³⁶ P. Travnicek,³¹ M. Trini,⁷² R. Ulrich,³⁴ M. Unger,^{9,34} M. Urban,⁴⁰ A. Valbuena-Delgado,²⁰ J. F. Valdés Galicia,¹³ I. Valiño,¹⁴ L. Valore,^{51,15} G. van Aar,⁴² P. van Bodegom,²⁶ A. M. van den Berg,⁸⁸ A. van Vliet,⁴² E. Varela,⁸² B. Vargas Cárdenas,¹³ G. Varner,⁷⁷ J. R. Vázquez,¹⁸ R. A. Vázquez,¹⁴ D. Veberič,³⁴ V. Verzi,⁶⁵ J. Vicha,³¹ M. Videla,¹¹ L. Villaseñor,⁴⁸ S. Vorobiov,⁷² H. Wahlberg,⁶⁸ O. Wainberg,^{11,12} D. Walz,⁴⁰ A. A. Watson,⁹⁸ M. Weber,⁷⁵ A. Weindl,³⁴ L. Wiencke,⁸⁰ H. Wilczyński,³⁷ T. Winchen,²⁵ D. Wittkowski,²⁵ B. Wundheiler,¹¹ S. Wykes,⁴² L. Yang,⁷² T. Yapici,⁵⁰ D. Yelos,^{12,11} E. Zas,¹⁴ D. Zavrtanik,^{72,71} M. Zavrtanik,^{71,72} A. Zepeda,⁸⁴ B. Zimmermann,⁷⁵ M. Ziolkowski,¹ Z. Zong,³⁰ and F. Zuccarello^{43,44}

(Pierre Auger Collaboration)*

¹Universität Siegen, Fachbereich 7 Physik—Experimentelle Teilchenphysik, Germany

²Laboratório de Instrumentação e Física Experimental de Partículas—LIP and Instituto Superior Técnico—IST, Universidade de Lisboa—UL, Portugal

³Osservatorio Astrofisico di Torino (INAF), Torino, Italy

⁴INFN, Sezione di Torino, Italy

⁵Fermi National Accelerator Laboratory, Batavia, Illinois, USA

⁶Laboratoire de Physique Nucléaire et de Hautes Energies (LPNHE), Universités Paris 6 et Paris 7, CNRS-IN2P3, France

⁷Universidade de São Paulo, Inst. de Física, São Paulo, Brazil

⁸Centro Atómico Bariloche and Instituto Balseiro (CNEA-UNCuyo-CONICET), Argentina

⁹New York University, New York, New York, USA

¹⁰Ohio State University, Columbus, Ohio, USA

¹¹Instituto de Tecnologías en Detección y Astropartículas (CNEA, CONICET, UNSAM), Centro Atómico Constituyentes, Comisión Nacional de Energía Atómica, Argentina

¹²Universidad Tecnológica Nacional—Facultad Regional Buenos Aires, Argentina

¹³Universidad Nacional Autónoma de México, Mexico

¹⁴Universidad de Santiago de Compostela, Spain

¹⁵INFN, Sezione di Napoli, Italy

¹⁶INFN, Sezione di L'Aquila, Italy

¹⁷Department of Physics and Astronomy, Lehman College, City University of New York, Bronx, New York, USA

¹⁸Universidad Complutense de Madrid, Spain

¹⁹University of Bucharest, Physics Department, Romania

²⁰Universidad Industrial de Santander, Colombia

²¹Observatorio Pierre Auger, Argentina

²²Observatorio Pierre Auger and Comisión Nacional de Energía Atómica, Argentina

²³University Politehnica of Bucharest, Romania

²⁴Karlsruhe Institute of Technology, Institut für Experimentelle Kernphysik (IEKP), Germany

²⁵Bergische Universität Wuppertal, Department of Physics, Germany, Germany

²⁶University of Adelaide, Australia

²⁷Laboratoire de Physique Subatomique et de Cosmologie (LPSC), Université Grenoble-Alpes, CNRS-IN2P3, France

²⁸Università Torino, Dipartimento di Fisica, Italy

²⁹Max-Planck-Institut für Radioastronomie, Bonn, Germany

³⁰Institut de Physique Nucléaire d'Orsay (IPNO), Université Paris 11, CNRS-IN2P3, France

³¹Institute of Physics (FZU) of the Academy of Sciences of the Czech Republic, Czech Republic

³²Università del Salento, Dipartimento di Matematica e Fisica “E. De Giorgi”, Italy

³³INFN, Sezione di Lecce, Italy

³⁴Karlsruhe Institute of Technology, Institut für Kernphysik (IKP), Germany

³⁵INFN Laboratori del Gran Sasso, Italy

³⁶Universidade Federal do Rio de Janeiro (UFRJ), Instituto de Física, Brazil

³⁷Institute of Nuclear Physics PAN, Poland

³⁸Colorado State University, Fort Collins, Colorado, USA

³⁹“Horia Hulubei” National Institute for Physics and Nuclear Engineering, Romania

⁴⁰RWTH Aachen University, III. Physikalisches Institut A, Germany

⁴¹Universidad de Granada and C.A.F.P.E., Spain

⁴²Institute for Mathematics, Astrophysics and Particle Physics (IMAPP), Radboud Universiteit, Nijmegen, Netherlands

⁴³Università di Catania, Dipartimento di Fisica e Astronomia, Italy

- ⁴⁴INFN, Sezione di Catania, Italy
- ⁴⁵Universidad Autónoma de Chiapas, Mexico
- ⁴⁶INFN, Sezione di Milano, Italy
- ⁴⁷Institute of Space Science, Romania
- ⁴⁸Universidad Michoacana de San Nicolás de Hidalgo, Mexico
- ⁴⁹Universidade Estadual de Campinas (UNICAMP), Brazil
- ⁵⁰Michigan Technological University, Houghton, Michigan, USA
- ⁵¹Università di Napoli “Federico II”, Dipartimento di Fisica, Italy
- ⁵²Pennsylvania State University, University Park, Pennsylvania, USA
- ⁵³Case Western Reserve University, Cleveland, Ohio, USA
- ⁵⁴University of Chicago, Chicago, Illinois, USA
- ⁵⁵SUBATECH, École des Mines de Nantes, CNRS-IN2P3, Université de Nantes, France
- ⁵⁶Station de Radioastronomie de Nançay, France
- ⁵⁷Università del Salento, Dipartimento di Ingegneria, Italy
- ⁵⁸Instituto de Astronomía y Física del Espacio (IAFE, CONICET-UBA), Argentina
- ⁵⁹Departamento de Física and Departamento de Ciencias de la Atmósfera y los Océanos, FCEyN, Universidad de Buenos Aires, Argentina
- ⁶⁰Universidade Federal Fluminense, Brazil
- ⁶¹Nationaal Instituut voor Kernfysica en Hoge Energie Fysica (NIKHEF), Netherlands
- ⁶²Universidade de São Paulo, Inst. de Física de São Carlos, São Carlos, Brazil
- ⁶³Universidad de Alcalá de Henares, Spain
- ⁶⁴Università di Roma “Tor Vergata”, Dipartimento di Fisica, Italy
- ⁶⁵INFN, Sezione di Roma “Tor Vergata”, Italy
- ⁶⁶Università dell’Aquila, Dipartimento di Chimica e Fisica, Italy
- ⁶⁷Universidade Federal do Paraná, Setor Palotina, Brazil
- ⁶⁸IFLP, Universidad Nacional de La Plata and CONICET, Argentina
- ⁶⁹Universität Hamburg, II. Institut für Theoretische Physik, Germany
- ⁷⁰Stichting Astronomisch Onderzoek in Nederland (ASTRON), Dwingeloo, Netherlands
- ⁷¹Experimental Particle Physics Department, J. Stefan Institute, Slovenia
- ⁷²Laboratory for Astroparticle Physics, University of Nova Gorica, Slovenia
- ⁷³Instituto de Física de Rosario (IFIR)—CONICET/U.N.R. and Facultad de Ciencias Bioquímicas y Farmacéuticas U.N.R., Argentina
- ⁷⁴Instituto de Tecnologías en Detección y Astropartículas (CNEA, CONICET, UNSAM) and Universidad Tecnológica Nacional—Facultad Regional Mendoza (CONICET/CNEA), Argentina
- ⁷⁵Karlsruhe Institute of Technology, Institut für Prozessdatenverarbeitung und Elektronik (IPE), Germany
- ⁷⁶University of Łódź, Poland
- ⁷⁷University of Hawaii, Honolulu, Hawaii, USA
- ⁷⁸Universidade Estadual de Feira de Santana (UEFS), Brazil
- ⁷⁹Palacky University, RCPTM, Czech Republic
- ⁸⁰Colorado School of Mines, Golden, Colorado, USA
- ⁸¹Universidade Federal do ABC (UFABC), Brazil
- ⁸²Benemérita Universidad Autónoma de Puebla (BUAP), Mexico
- ⁸³Università di Milano, Dipartimento di Fisica, Italy
- ⁸⁴Centro de Investigación y de Estudios Avanzados del IPN (CINVESTAV), Mexico
- ⁸⁵Louisiana State University, Baton Rouge, Louisiana, USA
- ⁸⁶University of New Mexico, Albuquerque, New Mexico, USA
- ⁸⁷Centro Brasileiro de Pesquisas Físicas (CBPF), Brazil
- ⁸⁸KVI—Center for Advanced Radiation Technology, University of Groningen, Netherlands
- ⁸⁹Universidade Federal de Pelotas, Brazil
- ⁹⁰University Prague, Institute of Particle and Nuclear Physics, Czech Republic
- ⁹¹Centro de Investigaciones en Láseres y Aplicaciones, CITEDEF and CONICET, Argentina
- ⁹²Northeastern University, Boston, Massachusetts, USA
- ⁹³Unidad Profesional Interdisciplinaria en Ingeniería y Tecnologías Avanzadas del Instituto Politécnico Nacional (UPIITA-IPN), Mexico
- ⁹⁴Universidade Federal da Bahia, Brazil
- ⁹⁵University of Nebraska, Lincoln, Nebraska, USA
- ⁹⁶INAF—Istituto di Astrofisica Spaziale e Fisica Cosmica di Palermo, Italy
- ⁹⁷Universidade de São Paulo, Escola de Engenharia de Lorena, Brazil
- ⁹⁸School of Physics and Astronomy, University of Leeds, Leeds, United Kingdom

(Received 23 April 2016; published 31 October 2016)

Ultrahigh energy cosmic ray air showers probe particle physics at energies beyond the reach of accelerators. Here we introduce a new method to test hadronic interaction models without relying on the absolute energy calibration, and apply it to events with primary energy 6–16 EeV ($E_{\text{CM}} = 110\text{--}170$ TeV), whose longitudinal development and lateral distribution were simultaneously measured by the Pierre Auger Observatory. The average hadronic shower is 1.33 ± 0.16 (1.61 ± 0.21) times larger than predicted using the leading LHC-tuned models EPOS-LHC (QGSJetII-04), with a corresponding excess of muons.

DOI: 10.1103/PhysRevLett.117.192001

Introduction.—For many years there have been hints that the number of muons in ultrahigh energy cosmic ray (UHECR) air showers is larger than predicted by hadronic interaction models, e.g., Ref. [1]. Most recently, the Pierre Auger Observatory [2] compared the muon number in highly inclined events to predictions using the two leading LHC-tuned hadronic event generators (HEGs) for air showers, QGSJet-II-04 [3,4], and EPOS-LHC [5,6]. The observed number of muons for 10^{19} eV primaries was found [7] to be 30%–80% higher than the models predict assuming the primary composition inferred from the depth-of-shower-maximum distribution for each given model [8,9], but the significance of the inferred muon excess is limited due to the uncertainty in the absolute energy calibration.

For a given primary energy and mass, the number of muons is sensitive to hadronic interactions. Typically about 25% of the final state energy in each hadronic interaction is carried by π^0 's, which immediately decay to two photons and thus divert energy from the hadronic cascade, which is the main source of muons, to the electromagnetic (EM) cascade. The hadronic cascade terminates when the energy of charged pions drops low enough that they decay before interacting, $O(100$ GeV). If the average fraction of EM energy per interaction were increased or decreased, or there were more or fewer generations of hadronic interactions in the cascade (which depends on the primary mass and properties of the final states such as multiplicity), the muon ground signal would be lower or higher. Therefore, a significant discrepancy between observed and predicted muon ground signal would indicate that the description of hadronic interactions is inaccurate, assuming that the composition can be properly understood.

There has been excellent recent progress in composition determination [8–10], which provides a valuable “prior” for modeling individual showers. Here we complement that progress with a new, more powerful approach to the muon analysis which removes the sensitivity to the absolute energy calibration. It is applicable to the entire data set of hybrid events: those events whose longitudinal profile (LP) is measured by the Pierre Auger Observatory’s fluorescence detector (FD) [2,11] at the same time the ground signal is measured with its surface detector (SD) [2,12].

The ground signal of an individual shower of a CR of given energy and mass depends primarily on the zenith

angle and the depth-of-shower-maximum, X_{max} , because together these determine the path length and thus attenuation of the electromagnetic and muonic components at ground. In order to most simply characterize a possible discrepancy between the predicted and observed properties of the air shower, we introduce an energy rescaling parameter, R_E , to allow for a possible shift in the FD energy calibration, and a multiplicative rescaling of the hadronic component of the shower by a factor R_{had} . R_E rescales the total ground signal of the event approximately uniformly, while R_{had} rescales only the contribution to the ground signal of inherently hadronic origin, which consists mostly of muons. Because the EM component of the shower is more strongly attenuated in the atmosphere than the muonic component, and the path length in the atmosphere varies as a function of zenith angle, R_E and R_{had} can be separately determined by fitting a sufficiently large sample of events covering a range of zenith angles.

In this analysis we test the consistency of the observed and predicted ground signal *event by event*, for a large sample of events covering a wide range of X_{max} and zenith angles. By selecting simulated events which accurately match the observed LP of each event, we largely eliminate the noise from shower-to-shower fluctuations in the ground signal due to fluctuations in X_{max} , while at the same time maximally exploiting the relative attenuation of the EM and muonic components of the shower.

The LP and lateral distribution of the ground signal of an illustrative event are shown in Fig. 1, along with a matching proton and iron simulated event; the ground signal size is measured in units of vertical equivalent muons (VEM), the calibrated unit of SD signal size [13]. Figure 1 (bottom) illustrates a general feature of the comparison between observed and simulated events: the ground signal of the simulated events is systematically smaller than the ground signal in the recorded events. Elucidating the nature of the discrepancy is the motivation for the present study.

The data we use for this study are the 411 hybrid events with $10^{18.8} < E < 10^{19.2}$ eV and zenith angle $0^\circ\text{--}60^\circ$ recorded between 1 January 2004 and 31 December 2012, which satisfy the event quality selection criteria in Refs. [14,15]. We thus concentrate on a relatively narrow energy range such that the mass composition changes rather little [8,9], while having adequate statistics. This energy range corresponds to an energy of 110 to 170 TeV in the

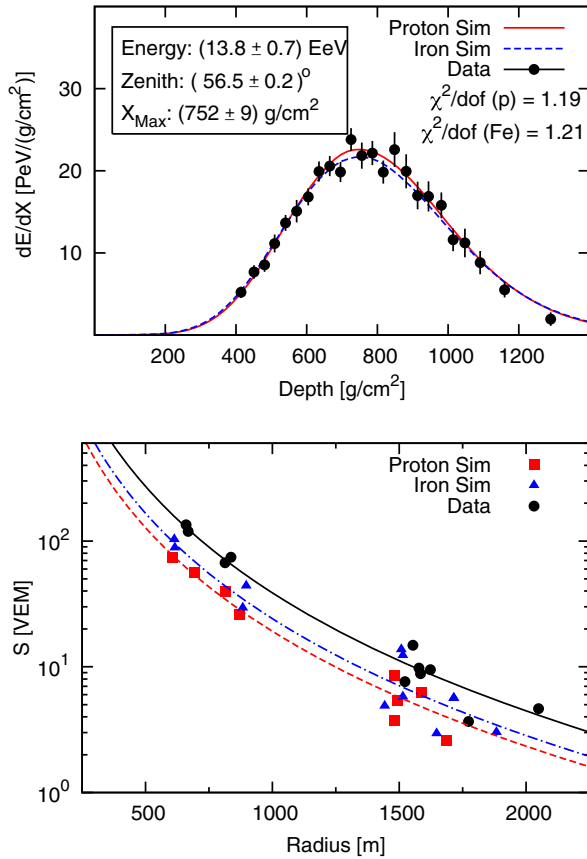


FIG. 1. Top: The measured longitudinal profile of an illustrative air shower with its matching simulated showers, using QGSJet-II-04 for proton (red solid) and iron (blue dashed) primaries. Bottom: The observed and simulated ground signals for the same event (p : red squares, dashed-line, Fe: blue triangles, dot-dash line) in units of vertical equivalent muons; curves are the lateral distribution function (LDF) fit to the signal.

center-of-mass reference frame of the UHECR and air nucleon, far above the LHC energy scale.

Figure 2 shows the ratio of $S(1000)$, the ground signal size at 1000 m from the shower core [2], for the events in our sample relative to that predicted for simulated events with matching zenith angle, depth-of-shower-maximum (X_{\max}) and calorimetric FD energy, for QGSJet-II-04 [3] and EPOS-LHC [5]. For each HEG, the analysis is done using the composition mix which reproduces the observed X_{\max} distribution [8,9]; we also show the result for pure protons for comparison. The discrepancy between a measured and simulated $S(1000)$ evident in Fig. 2 is striking, at all angles and for both HEGs, and for both the mixed composition and pure proton cases.

The zenith angle dependence of the discrepancy is the key to allowing R_E and R_{had} to be separated. As seen in Fig. 3, the ground signal from the hadronic component is roughly independent of zenith angle, whereas that of the EM component falls with $\sec(\theta)$, so that to reproduce the rise seen in Fig. 2, the hadronic component must be

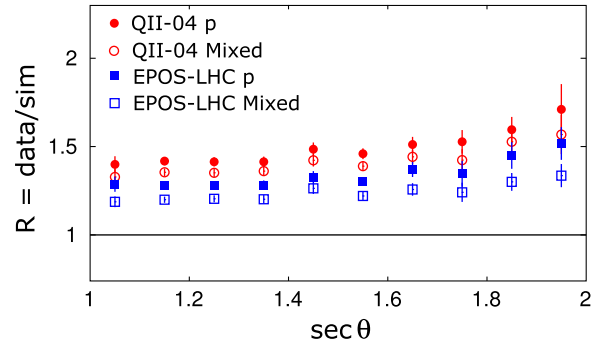


FIG. 2. The average ratio of $S(1000)$ for observed and simulated events as a function of zenith angle, for mixed or pure proton compositions.

increased with little or no modification of the EM component. This will be quantified below.

The analysis relies on there being no significant zenith-angle-dependent bias in the determination of the SD and FD signals. The accuracy of the detector simulations as a function of zenith angle in the 0° – 60° range of the study here, and hence the absence of a zenith-angle-dependent bias in the SD reconstruction, has been extensively validated with muon test data [16]. The absence of zenith-angle dependence in the normalization of the FD signal follows from the zenith-angle independence of $E_{\text{FD}}/E_{\text{SD}}$ of individual hybrid events.

Production of simulated events.—The first step of the analysis is to generate a set of Monte Carlo (MC) events, to find simulated events matching the LPs of the data events. The MC air-shower simulations are performed using the SENECA simulation code [17], with FLUKA [19] as the low-energy HEG. Simulation of the surface detector response is performed with GEANT4 [20] within the software framework Offline [21] of the Auger Observatory. We produce showers matching each data event, with both HEGs and for

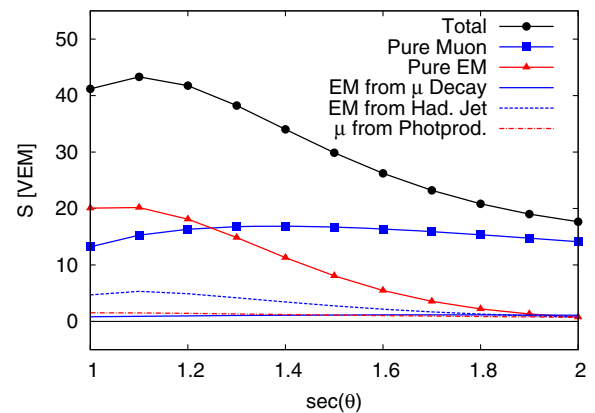


FIG. 3. The contributions of different components to the average signal as a function of zenith angle, for stations at 1 km from the shower core, in simulated 10 EeV proton air showers illustrated for QGSJet-II-04.

all four primary cosmic-ray types (proton, helium, nitrogen, and iron nuclei), as follows:

Repeatedly generate showers with the measured geometry and calorimetric energy of the given data event, reconstructing the LP and determining the X_{\max} value until 12 showers having the same X_{\max} value as the real event (within the reconstruction uncertainty) have been produced, or stopping after 600 tries. For data events whose X_{\max} cannot be matched with all primary types, the analysis is done using only those primaries that give 12 events at this stage, in 600 tries [22].

Repeat the simulation of these 12 showers at very high resolution, and select the 3 which best reproduce the observed longitudinal profile based on the χ^2 fit. For each of the 3 selected showers, do a full surface detector simulation and generate SD signals for comparison with the data. From these detailed simulations of 3 showers that match the full LP of the data event, determine the hadronic component of the simulated ground signal and the shower-to-shower variance.

The choices of 12 and 3 showers in the two stages above assure, respectively, that (i) the LPs of the final simulated data set fit the real data with a χ^2 distribution that is comparable to that found in a Gaisser-Hillas fit to the data itself, and (ii) that the variance within the simulated events for a given shower is smaller than the shower-to-shower fluctuations in real events. More than 10^7 showers must be simulated to create the analysis library of well-fitting simulated showers for the 411 hybrid events of the data set. A high-quality fit to the LP is found for all events, for at least one primary type.

Quantifying the discrepancy.—The history of all muons and EM particles (e^\pm and γ 's) reaching the ground is tracked during simulation, following the description in Ref. [23]. Most muons come from π^\pm or K decay and most EM particles from π^0 decay. The portion of EM particles that are produced by muons through decay or radiative processes, and by low-energy π^0 's, are attributed to the hadronic signal, S_{had} ; muons that are produced through photoproduction are attributed to the electromagnetic signal, S_{EM} . The relative importance of the different components varies with zenith angle, as illustrated in Fig. 3. Once S_{EM} and S_{had} are known for a given shower i , with assumed primary mass j , the rescaled simulated $S(1000)$ can be written as

$$S_{\text{resc}}(R_E, R_{\text{had}})_{i,j} \equiv R_E S_{\text{EM},i,j} + R_{\text{had}} R_E^\alpha S_{\text{had},i,j}. \quad (1)$$

The linear scaling of the EM contribution with R_E is obvious, as is the factor R_{had} for the hadronic contribution. The factor R_E^α reflects the fact that the hadronic signal increases slower than linearly with energy, since higher energy events require more stages in the shower cascade before the pions have low enough energy to decay to muons rather than re-interact, and at each stage, energy is removed

from the hadronic cascade. The value of α is a prediction of the HEG and depends also on mass; in practice, both EPOS and QGSJet-II simulations find $\alpha \approx 0.9$, relatively independently of composition [24]. We investigated the sensitivity of our conclusions to the possibility that α predicted by the models is incorrect, and find its potential effect is small enough to be ignored for the present analysis [25].

The best fit values of R_E and R_{had} are determined by maximizing the likelihood function $\prod_i P_i$, where the index i runs over each event in the data set and the contribution of the i th event is

$$P_i = \sum_j \frac{p_j(X_{\max,i})}{\sqrt{2\pi\sigma_{i,j}^2}} \exp \left[\frac{-(S_{\text{resc}}(R_E, R_{\text{had}})_{i,j} - S(1000)_i)^2}{2\sigma_{i,j}^2} \right]. \quad (2)$$

The index j labels the different possible primaries (p , He, N, and Fe), and $p_j(X_{\max,i})$ is the prior on the probability that an event with $X_{\max,i}$ has mass j , given the mass fractions f_j in the interval $10^{19 \pm 0.2}$ eV (see Ref. [8] for the fit to the observed X_{\max} distribution for each HEG):

$$p_j(X_{\max}) = f_j \mathcal{P}_j(X_{\max}) / \sum_j f_j \mathcal{P}_j(X_{\max}), \quad (3)$$

where $\mathcal{P}_j(X_{\max})$ is the probability density of observing X_{\max} for primary type j , for the given HEG. The variance entering Eq. (2) includes (a) measurement uncertainty of typically 12%, from the uncertainty in the reconstruction of $S(1000)$, the calorimetric energy measurement, and the uncertainty in the X_{\max} scale, as well as (b) the variance in the ground signals of showers with matching LPs due to shower-to-shower fluctuations (ranging from typically 16% for proton-initiated showers to 5% for iron-initiated showers) and (c) the uncertainty in separating S_μ and S_{EM} in the simulation, and from the limited statistics of having only three simulated events (typically 10% for proton-initiated showers and 4% for iron-initiated showers).

Results and discussion.—Table I gives the values of R_E and R_{had} which maximize the likelihood of the observed ground signals, for the various combinations of HEGs and compositions considered. The systematic uncertainties in the reconstruction of X_{\max} , E_{FD} and $S(1000)$ are propagated through the analysis by shifting the reconstructed central values by their one-sigma systematic uncertainties.

TABLE I. R_E and R_{had} with statistical and systematic uncertainties, for QGSJet-II-04 and EPOS-LHC.

| Model | R_E | R_{had} |
|--------------|--------------------------|--------------------------|
| QII-04 p | $1.09 \pm 0.08 \pm 0.09$ | $1.59 \pm 0.17 \pm 0.09$ |
| QII-04 mixed | $1.00 \pm 0.08 \pm 0.11$ | $1.61 \pm 0.18 \pm 0.11$ |
| EPOS p | $1.04 \pm 0.08 \pm 0.08$ | $1.45 \pm 0.16 \pm 0.08$ |
| EPOS mixed | $1.00 \pm 0.07 \pm 0.08$ | $1.33 \pm 0.13 \pm 0.09$ |

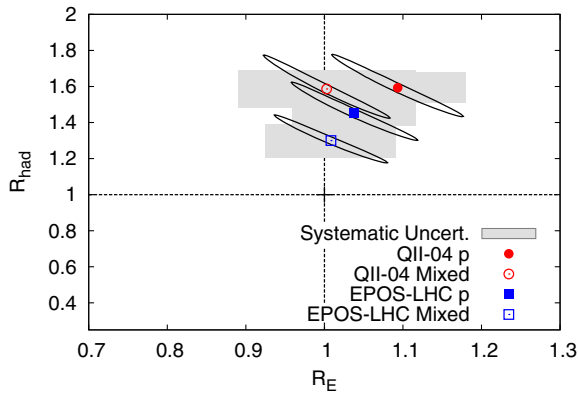


FIG. 4. Best-fit values of R_E and R_{had} for QGSJet-II-04 and EPOS-LHC, for pure proton (solid circle, square) and mixed composition (open circle, square). The ellipses and gray boxes show the $1\text{-}\sigma$ statistical and systematic uncertainties.

Figure 4 shows the one-sigma statistical uncertainty ellipses in the $R_E - R_{\text{had}}$ plane; the outer boundaries of propagating the systematic errors are shown by the gray rectangles.

The values of R_{had} needed in the models are comparable to the corresponding muon excess detected in highly inclined air showers [7], as is expected because at high zenith angle the nonhadronic contribution to the signal (shown with red curves in Fig. 3) is much smaller than the hadronic contribution. However, the two analyses are not equivalent because a muon excess in an inclined air shower is indistinguishable from an energy rescaling, whereas in the present analysis the systematic uncertainty of the overall energy calibration enters only as a higher-order effect. Thus, the significance of the discrepancy between data and model prediction is now more compelling, growing from 1.38 (1.77) sigma to 2.1 (2.9) sigma, respectively, for EPOS-LHC (QGSJet II-04), adding statistical and systematic errors from Fig. 6 of Ref. [7] and Table I, in quadrature.

The signal deficit is smallest (the best-fit R_{had} is the closest to unity) with EPOS-LHC and mixed composition. This is because, for a given mass, the muon signal is $\approx 15\%$ larger for EPOS-LHC than QGSJet-II-04 [26], and in addition the mean primary mass is larger when the X_{max} data are interpreted with EPOS rather than with QGSJet-II [9].

Within the event ensemble used in this study, there is no evidence of a larger event-to-event variance in the ground signal for fixed X_{max} than predicted by the current models. This means that the muon shortfall cannot be attributed to an exotic phenomenon producing a very large muon signal in only a fraction of events, such as could be the case if microscopic black holes were being produced at a much-larger-than-expected rate [27,28].

Summary.—We have introduced a new method to study hadronic interactions at ultrahigh energies, which

minimizes reliance on the absolute energy determination and improves precision by exploiting the information in individual hybrid events. We applied it to hybrid showers of the Pierre Auger Observatory with energies 6–16 EeV ($E_{\text{CM}} = 110$ to 170 TeV) and zenith angle 0° – 60° , to quantify the disparity between state-of-the-art hadronic interaction modeling and observed UHECR atmospheric air showers. We considered the simplest possible characterization of the model discrepancies, namely, an overall rescaling of the hadronic shower, R_{had} , and we allow for a possible overall energy calibration rescaling, R_E .

No energy rescaling is needed: $R_E = 1.00 \pm 0.10$ for the mixed composition fit with EPOS-LHC, and $R_E = 1.00 \pm 0.14$ for QGSJet II-04, adding systematic and statistical errors in quadrature. This uncertainty on R_E is of the same order of magnitude as the 14% systematic uncertainty of the energy calibration [14].

We find, however, that the observed hadronic signal in these UHECR air showers is significantly larger than predicted by models tuned to fit accelerator data. The best case, EPOS-LHC with mixed composition, requires a hadronic rescaling of $R_{\text{had}} = 1.33 \pm 0.16$ (statistical and systematic uncertainties combined in quadrature), while for QGSJet II-04, $R_{\text{had}} = 1.61 \pm 0.21$. It is not yet known whether this discrepancy can be explained by some incorrectly modeled features of hadron collisions, possibly even at low energy, or may be indicative of the onset of some new phenomenon in hadronic interactions at ultrahigh energy. Proposals of the first type include a higher level of production of baryons [26] or vector mesons [29] (see Ref. [30] for a recent review of the many constraints to be satisfied), while proposals for possible new physics are discussed in Refs. [28,31,32].

The discrepancy between models and nature can be elucidated by extending the present analysis to the entire hybrid data set above $10^{18.5}$ eV, to determine the energy dependence of R_E and R_{had} . In addition, the event-by-event analysis introduced here can be generalized to include other observables with complementary sensitivity to hadronic physics and composition, e.g., muon production depth [33], risetime [34], and slope of the LDF.

AugerPrime, the anticipated upgrade of the Pierre Auger Observatory [35], will significantly improve our ability to investigate hadronic interactions at ultrahigh energies, by separately measuring the muon and EM components of the ground signal.

The successful installation, commissioning, and operation of the Pierre Auger Observatory would not have been possible without the strong commitment and effort from the technical and administrative staff in Malargüe.

We are very grateful to the following agencies and organizations for financial support: Comisión Nacional de Energía Atómica, Agencia Nacional de Promoción Científica y Tecnológica (ANPCyT), Consejo Nacional de Investigaciones Científicas y Técnicas (CONICET),

Gobierno de la Provincia de Mendoza, Municipalidad de Malargüe, NDM Holdings and Valle Las Leñas, in gratitude for their continuing cooperation over land access, Argentina; the Australian Research Council; Conselho Nacional de Desenvolvimento Científico e Tecnológico (CNPq), Financiadora de Estudos e Projetos (FINEP), Fundação de Amparo à Pesquisa do Estado de Rio de Janeiro (FAPERJ), São Paulo Research Foundation (FAPESP) Grants No. 2010/07359-6 and No. 1999/05404-3, Ministério de Ciência e Tecnologia (MCT), Brazil; Grant No. MSMT-CR LG15014, No. LO1305, and No. LM2015038, and the Czech Science Foundation Grant No. 14-17501S, Czech Republic; Centre de Calcul IN2P3/CNRS, Centre National de la Recherche Scientifique (CNRS), Conseil Régional Ile-de-France, Département Physique Nucléaire et Corpusculaire (PNC-IN2P3/CNRS), Département Sciences de l'Univers (SDU-INSU/CNRS), Institut Lagrange de Paris (ILP) Grant No. LABEX ANR-10-LABX-63, within the Investissements d'Avenir Programme Grant No. ANR-11-IDEX-0004-02, France; Bundesministerium für Bildung und Forschung (BMBF), Deutsche Forschungsgemeinschaft (DFG), Finanzministerium Baden-Württemberg, Helmholtz Alliance for Astroparticle Physics (HAP), Helmholtz-Gemeinschaft Deutscher Forschungszentren (HGF), Ministerium für Innovation, Wissenschaft und Forschung des Landes Nordrhein-Westfalen, Ministerium für Wissenschaft, Forschung und Kunst, Baden-Württemberg, Germany; Istituto Nazionale di Fisica Nucleare (INFN), Istituto Nazionale di Astrofisica (INAF), Ministero dell'Istruzione, dell'Università e della Ricerca (MIUR), Gran Sasso Center for Astroparticle Physics (CFA), CETEMPS Center of Excellence, Ministero degli Affari Esteri (MAE), Italy; Consejo Nacional de Ciencia y Tecnología (CONACYT) No. 167733, Mexico; Universidad Nacional Autónoma de México (UNAM), PAPIIT DGAPA-UNAM, Mexico; Ministerie van Onderwijs, Cultuur en Wetenschap, Nederlandse Organisatie voor Wetenschappelijk Onderzoek (NWO), Stichting voor Fundamenteel Onderzoek der Materie (FOM), Netherlands; National Centre for Research and Development, Grants No. ERA-NET-ASPERA/01/11 and No. ERA-NET-ASPERA/02/11, National Science Centre, Grants No. 2013/08/M/ST9/00322, No. 2013/08/M/ST9/00728 and No. HARMONIA 5-2013/10/M/ST9/00062, Poland; Portuguese national funds and FEDER funds within Programa Operacional Factores de Competitividade through Fundação para a Ciência e a Tecnologia (COMPETE), Portugal; Romanian Authority for Scientific Research ANCS, CNDI-UEFISCDI partnership projects Grants No. 20/2012 and No. 194/2012, Grants No. 1/ASPERA2/2012 ERA-NET, No. PN-II-RU-PD-2011-3-0145-17 and No. PN-II-RU-PD-2011-3-0062, the Minister of National Education, Programme Space

Technology and Advanced Research (STAR), Grant No. 83/2013, Romania; Slovenian Research Agency, Slovenia; Comunidad de Madrid, Fondo Europeo de Desarrollo Regional (FEDER) funds, Ministerio de Educación y Ciencia, Xunta de Galicia, European Community 7th Framework Program, Grant No. FP7-PEOPLE-2012-IEF-328826, Spain; Science and Technology Facilities Council, United Kingdom; Department of Energy, Contracts No. DE-AC02-07CH11359, No. DE-FR02-04ER41300, No. DE-FG02-99ER41107 and No. DE-SC0011689, National Science Foundation, Grants No. 0450696, and The Grainger Foundation, USA; Marie Curie-IRSES/EPLANET, European Particle Physics Latin American Network, European Union 7th Framework Program, Grant No. PIRSES-2009-GA-246806; and UNESCO.

*auger_spokespersons@fnal.gov;

<http://www.auger.org>

†Also at Deutsches Elektronen-Synchrotron (DESY), Zeuthen, Germany.

‡Also at Vrije Universiteit Brussels, Brussels, Belgium.

- [1] T. Abu-Zayyad *et al.* (HiRes-MIA Collaboration), *Phys. Rev. Lett.* **84**, 4276 (2000).
- [2] A. Aab *et al.* (Pierre Auger Collaboration), *Nucl. Instrum. Methods Phys. Res., Sect. A* **798**, 172 (2015).
- [3] S. Ostapchenko, *Phys. Rev. D* **83**, 014018 (2011).
- [4] S. Ostapchenko, *Nucl. Phys. B, Proc. Suppl.* **151**, 143 (2006).
- [5] T. Pierog, Iu. Karpenko, J. M. Katzy, E. Yatsenko, and K. Werner, *Phys. Rev. C* **92**, 034906 (2015).
- [6] K. Werner, F.-M. Liu, and T. Pierog, *Phys. Rev. C* **74**, 044902 (2006).
- [7] A. Aab *et al.* (Pierre Auger Collaboration), *Phys. Rev. D* **91**, 032003 (2015).
- [8] A. Aab *et al.* (Pierre Auger Collaboration), *Phys. Rev. D* **90**, 122005 (2014).
- [9] A. Aab *et al.* (Pierre Auger Collaboration), *Phys. Rev. D* **90**, 122006 (2014).
- [10] M. Unger *et al.* (Pierre Auger and Telescope Array Collaborations), Report of the Working Group on the Composition of Ultra-High Energy Cosmic Rays, *Proceedings of the 34th ICRC, The Hague, The Netherlands, 2015*, PoS(ICRC2015), p. 307, [arXiv:1511.02103](https://arxiv.org/abs/1511.02103).
- [11] J. Abraham *et al.* (Pierre Auger Collaboration), *Nucl. Instrum. Methods Phys. Res., Sect. A* **620**, 227 (2010).
- [12] J. Abraham *et al.* (Pierre Auger Collaboration) **523**, 50 (2004).
- [13] X. Bertou *et al.*, *Nucl. Instrum. Methods Phys. Res., Sect. A* **568**, 839 (2006).
- [14] V. Verzi *et al.* (Pierre Auger Collaboration), *Proceedings of the 33rd International Cosmic Ray Conference (ICRC), Rio de Janeiro, Brazil, 2013* edited by R. C. Shellard (2013), paper 0928, http://www.cbpf.br/~icrc2013/proc_icrc2013.html.

- [15] R. Pesce *et al.* (Pierre Auger Collaboration), *Proceedings of the 32nd International Cosmic Ray Conference (ICRC), Beijing, China* (2011), Vol. 2, p. 214.
- [16] P. Assis *et al.* (Pierre Auger Collaboration), *Proceedings of the 34th International Cosmic Ray Conference (ICRC), The Hague, Netherlands, 2015*, PoS(ICRC2015), p. 620.
- [17] SENECA is an efficient air shower generator which produces fully 3D showers that agree with the widely used CORSIKA [18] code, on both the ensemble and shower-by-shower level, while being significantly faster; for details see H.-J. Drescher and G. Farrar, *Phys. Rev. D* **67**, 116001 (2003); J. Allen, H. J. Drescher, and G. Farrar, arXiv:0708.2892.
- [18] D. Heck, J. Knapp, J. N. Capdevielle, G. Schatz, and T. Thouw, Forschungszentrum Karlsruhe Report No. FZKA 6019, 1998.
- [19] G. Battistoni, F. Cerutti, A. Fassò, A. Ferrari, S. Muraro, J. Ranft, S. Roesler, and P. R. Sala, *AIP Conf. Proc.* **896**, 31 (2007).
- [20] S. Agostinelli *et al.*, *Nucl. Instrum. Methods Phys. Res., Sect. A* **506**, 250 (2003).
- [21] S. Argiro, S. L. C. Barroso, J. Gonzalez, L. Nellen, T. Paul, T. A. Porter, L. Prado Jr., M. Roth, R. Ulrich, and D. Veberič, *Nucl. Instrum. Methods Phys. Res., Sect. A* **580**, 1485 (2007).
- [22] 261 of the 411 events have an X_{\max} value so deep or shallow that the LP cannot be reproduced with all primaries for both HEGs, e.g., 209 (230) events cannot be described as Fe, and 32 (10) cannot be described as a proton, in EPOS-LHC (QGSJetII-04), respectively.
- [23] M. Ave *et al.*, *Proceedings of the 32nd International Cosmic Ray Conference (ICRC), Beijing, China* (2011), p. 178.
- [24] J. Alvarez-Muñiz, R. Engel, T. K. Gaisser, J. A. Ortiz, and T. Stanev, *Phys. Rev. D* **66**, 033011 (2002).
- [25] The potential sensitivity to α arises in spite of the narrow primary energy range, because individual nucleons in a primary of mass A carry energy E/A . To investigate this we let $R_{\text{had}}(A, E) \equiv [(E/10 \text{ EeV})/A]^{\delta\alpha} R_{\text{had}}$, where R_{had} is the rescaling factor for proton primaries at 10^{19} eV. We take $\delta\alpha = 0.01$ as the fiducial value, motivated by Ref. [31], which achieves $R_{\text{had}} \approx 1.3$ by converting π^0 's and η 's to other mesons, resulting in $\delta\alpha = 0.0135$ for EPOS and 0.01–0.02 for QGSJet. Reanalyzing with $\delta\alpha = 0(0.02)$, R_E changes negligibly, and $R_{\text{had}} \rightarrow 1.30(1.37)$ for EPOS.
- [26] T. Pierog, *Eur. Phys. J. Web Conf.* **52**, 03001 (2013).
- [27] J. L. Feng and A. D. Shapere, *Phys. Rev. Lett.* **88**, 021303 (2001).
- [28] G. R. Farrar and J. D. Allen, *Eur. Phys. J. Web Conf.* **53**, 07007 (2013).
- [29] H. J. Drescher, *Phys. Rev. D* **77**, 056003 (2008).
- [30] R. Engel, Proceedings of the 34th International Cosmic Ray Conference (ICRC), The Hague, Netherlands (to be published); <https://indico.cern.ch/event/344485/contribution/1384>.
- [31] J. Allen and G. Farrar, Proceedings of the 33rd International Cosmic Ray Conference (ICRC), Rio de Janeiro, Brazil, 2013, paper 1182; arXiv:1307.7131.
- [32] J. Alvarez-Muñiz, L. Cazon, R. Conceição, J. D. de Deus, C. Pajares, and M. Pimenta, arXiv:1209.6474.
- [33] A. Aab *et al.* (Pierre Auger Collaboration), *Phys. Rev. D* **91**, 032003 (2015); **91**, 059901(E) (2015).
- [34] A. A. Watson and J. G. Wilson, *J. Phys. A* **7**, 1199 (1974); A. Aab *et al.* (Pierre Auger Collaboration), *Phys. Rev. D* **93**, 072006 (2016).
- [35] A. Aab *et al.* (Pierre Auger Collaboration), arXiv:1604.03637.